Analytical Methods

www.rsc.org/methods
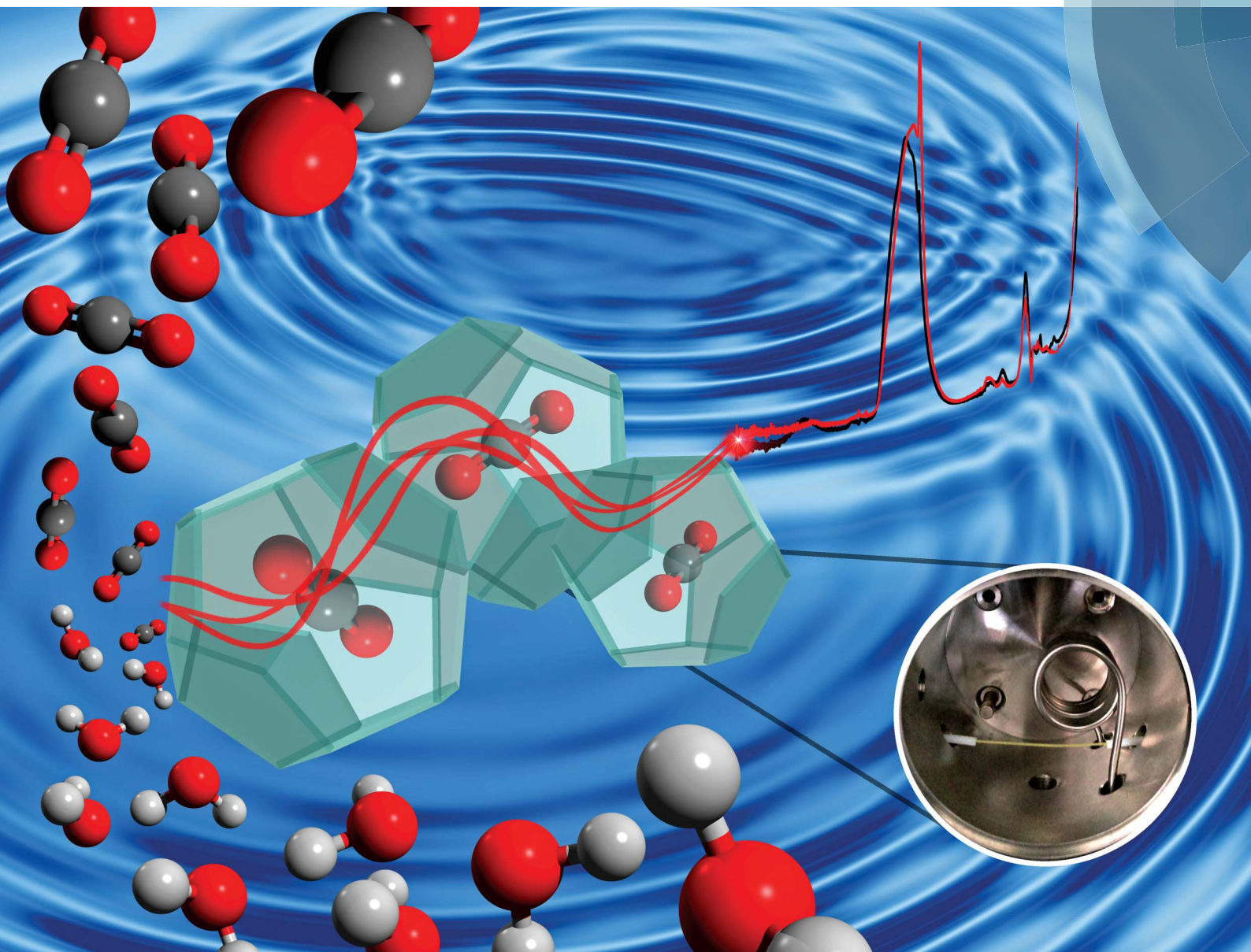
ROYAL SOCIETY
OF **CHEMISTRY**

175 YEARS

PAPER
Boris Mizaikoff *et al.*
In situ monitoring of additives during CO₂ gas hydrate formation

Analytical Methods

PAPER

In situ monitoring of additives during CO$_2$ gas hydrate formation

M. Schwenk,[a] A. Katzir[b] and B. Mizaikoff*[a]

Research activities on the reduction of carbon dioxide emissions *via* effective carbon capture and storage (CCS) techniques are steadily increasing with the concept of storing CO$_2$ as hydrates among the most prominently discussed strategies. The present study utilizes mid-infrared (MIR) fiber-optic evanescent field sensing techniques as a promising *in situ* monitoring tool for investigation of molecular changes occurring during CO$_2$ hydrate formation. The identification and evaluation of characteristic IR absorption features associated with additive molecules (here, THF and SDS) and their changes during hydrate formation were pronounced *via* studies in D$_2$O next to H$_2$O as the hydrate-forming matrix. By correlating IR-spectroscopic data with continuously recorded pressure and temperature traces, hypotheses on the involvement and promoting effect of such additives during carbon dioxide gas hydrate formation were experimentally consolidated.

1 Introduction

Gas hydrates are crystalline compounds comprising structured water cavities hosting small guest molecules. Different hydrate structures result from combinations of individual cages. In the case of natural gas hydrates, three distinctive structures have been identified: cubic sI, cubic sII, and hexagonal sH. The capability of trapping increasingly larger guest molecules is associated with increasing cage dimensions from sI to sH.[1,2]

CO$_2$ gas hydrates are known to form the cubic structure sI characterized by a unit cell comprising two smaller dodecahedral (5^{12}) cages, and six larger tetrakaidecahedral ($5^{12}6^2$) cages formed by 46 water molecules.[1,2] At full occupation, this leads to a composition of CO$_2 \times 5.75$ H$_2$O. However, it is commonly agreed that nearly all the large cages are being occupied along with a fraction of the small cages, thereby leading to a hydrate composition of CO$_2 \times 5.75$–7.66 H$_2$O.[3,4]

Research interest in CO$_2$ hydrates is frequently associated with the potential storage of CO$_2$ as gas hydrates, and/or the simultaneous production of methane during a hydrate exchange process (*i.e.*, methane stored in gas hydrates is retrieved, while sequestering CO$_2$ into the ice structure).[5–8] Another process of significant interest relates to reducing greenhouse gas emission by formation of gas hydrates as a novel strategy for capturing/separating CO$_2$ from synthesis or flue gases.[9–12] The usage of specific additives in hydrate research to influence the formation conditions is widely accepted in this context. Generally, such additives are divided into

thermodynamic and kinetic promoters. Tetrahydrofurane (THF) has proven to be an effective thermodynamic promoter *via* its ability to alter the equilibrium conditions of hydrate formation towards higher temperatures and/or lower pressures.[13,14] In the field of kinetic promotors, the anionic tenside sodium dodecyl sulphate (SDS) positively influences the hydrate/water conversion ratio, as well as the growth rate for hydrocarbon hydrates.[15,16] Also, the combined use of both additives affecting CO$_2$ hydrate formation has led to promising results.[17–19] However, the underlying mechanisms of the promoting effect remain under debate requiring further research to elucidate the governing processes. Commonly, two main principles of additive-assisted hydrate formation are discussed, especially for kinetic additives such as SDS: (i) capillary-driven mechanisms,[15,20] and (ii) promotion *via* surfactant micelle formation.[16]

In order to gain further insight into the process of gas hydrate formation, innovative monitoring techniques are demanded. Despite their exquisite molecular selectivity, IR-based spectroscopic and sensing techniques have to date rarely been applied in hydrate research, as reported within only a few publications.[21–29] Bertie and Othen pioneered this field by applying IR spectroscopy to investigate ethylene oxide hydrate in the spectral window of 4000–20 cm^{-1}.[21,22] Later, Fleyfel and Devlin proved that two separate peaks for CO$_2$ in the small and large cages of sI hydrate structures may be identified within thin films of the CO$_2$ hydrate, which was epitaxially grown on ethylene oxide hydrate. The absorption signals were evident at 2347 cm^{-1} and 2338 cm^{-1} at a temperature of 135 K for the small dodecahedral and the large tetrakaidecahedral cages, respectively.[25] Later, Kumar *et al.* applied infrared attenuated total reflection (IR-ATR) spectroscopy to investigate thin films of

[a]Institute of Analytical and Bioanalytical Chemistry, Ulm University, Albert-Einstein-Allee 11, Ulm 89081, Germany. E-mail: boris.mizaikoff@uni-ulm.de
[b]The School of Physics and Astronomy, Tel Aviv University, Tel Aviv 69978, Israel

CO_2 hydrate, and consolidated the results reported at that time *via* absorption signals at 2347 cm^{-1} and 2336 cm^{-1} at −50 °C for small and large cages, respectively.[26] In order to gain *in situ* access, while actually monitoring hydrate formation in real time, the group of Mizaikoff successfully applied for the first time IR fiber-optic evanescent field spectroscopy (FEFS) based on the principles of IR-ATR in order to investigate hydrocarbon gas hydrate formation.[30,31] These studies revealed that the observed IR-spectroscopic changes of water could be associated with gas hydrate formation processes. The evaluation of the infrared absorption signatures of SDS lead to the suggestion of a mechanism for the promotion of propane hydrate formation *via* SDS.[31] Although IR spectroscopy remains a rarely applied analytical technique, the achieved results clearly indicate that its potential is underrated in gas hydrate research and that IR-based techniques are indeed viable options for fundamentally understanding and molecularly deciphering gas hydrate formation processes.

The present study focuses on the application of fiber-optic IR-ATR sensing technologies for *in situ* monitoring of CO_2-containing gas hydrates formed in water and deuterated water in the presence of relevant additives (*i.e.*, THF and SDS). The obtained spectral data were correlated with simultaneously recorded pressure and temperature traces, which add additional physical information to the chemical data derived from the IR-spectra.

2   Results and discussion

CO_2 hydrates produced during the present study were analyzed both non-spectroscopically, by recording pressure/temperature (pT) traces, and *via* continuous *in situ* MIR-FEFS monitoring. Accordingly, thus obtained IR spectra were correlated with the information provided *via* the pT traces.

2.1   Pressure/temperature monitoring of CO_2 gas hydrates

Initial hydrate formation is indicated *via* a sharp temperature peak due to the exothermic nature of the crystallization process. Fig. 1 shows typical pT-traces *versus* the time for CO_2 gas hydrate experiments. For clarity, only the first 50 hours are displayed for an experiment using H_2O (Fig. 1a) and D_2O (Fig. 1b) as the background matrix, respectively.

The initial pressure reduction can be attributed to increased gas solubilization with decreasing temperature during the cooling phase. After approx. 3 hours, the experiment in H_2O (Fig. 1a) showed a sharp temperature peak (1) of 7.6 °C, thereby indicating initiation of gas hydrate nucleation. Subsequently, the pressure dropped (2) due to the incorporation of gas into the clathrate structure. The gas supply was activated several times throughout the experiment in order to replenish the already consumed gas (3) in the system until a characteristic pressure drop was not observable anymore. The temperature was kept at approx. 5 °C during the entire experiment. The experiment using D_2O as the matrix revealed similar behaviour (Fig. 1b). The sharp temperature peak (1) occurred here after approx. 2.8 hours at 8.5 °C. The subsequent pressure drop (2) was more
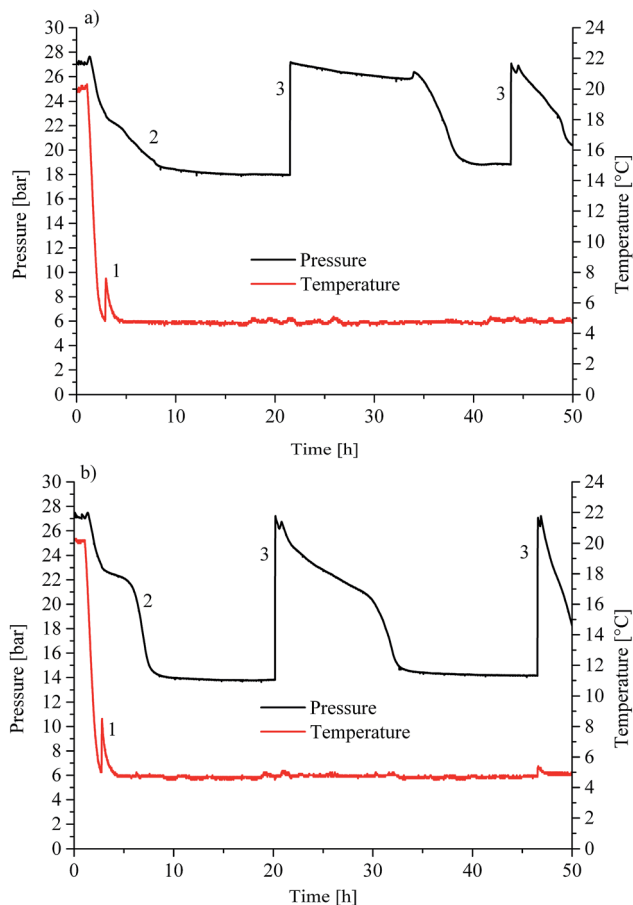

Fig. 1 Pressure/temperature *vs.* time for (a) CO_2 hydrate experiment in H_2O and (b) in D_2O as the bulk matrix.

pronounced compared to that of the H_2O experiment. The lattice constant for deuterated methane hydrate is up to 0.15% larger than that for the hydrogenated species. This increase may lead to higher cage occupancy in the case of deuterated CO_2 hydrates.[32] This would give rise to an increased uptake of gas, and a lower resulting pressure during the formation (Fig. 1b). Subsequently, both experiments show additional temperature peaks, which indicate further nucleation (not shown in Fig. 1). Gas consumption during the first nucleation period ceased after approx. 15 and approx. 10 hours for H_2O and D_2O, respectively (Fig. 1a and b). During the present experiments, first nucleation occurred nearly after the same time even though in general gas hydrate nucleation is supposed to be a stochastic event. Using *in situ* injection of THF, Ricaurte *et al.* could successfully eliminate the stochasticity of hydrate crystallisation enforcing nucleation on the system.[33] In order to facilitate hypothesizing on the hydrate species forming during the first nucleation phase, pressure *vs.* temperature data of both experiments (Fig. 1a and b) are presented in comparison with equilibrium curves for pure CO_2 hydrate derived from the literature (Adisasmito *et al.* 1991[34]), and CO_2 hydrate in the presence of 3.8 wt% THF (Delahaye *et al.* 2006[13]) in Fig. 2.

For clarity, Fig. 2 only shows the pressure *vs.* temperature traces for part of the cooling phase and the first nucleation
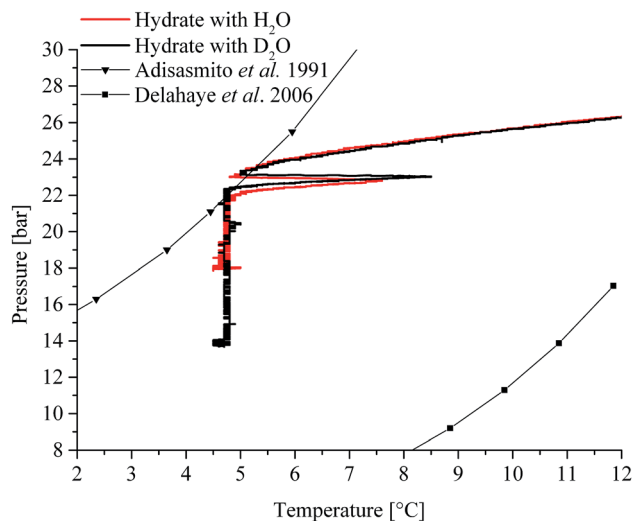
Fig. 2 Pressure *vs.* temperature data obtained during the present study in comparison with equilibrium data reported in the literature (pressure and temperature data have been converted to bar and °C, respectively).[13,34]

phase observed during the experiments depicted in Fig. 1. It is evident that the finally achieved pressure value is lower in the case of D_2O, as previously stated. In a system with THF and CO_2, the initially formed hydrate is apparently a mixed species comprising THF and CO_2.[17] The fact that for both experiments the initial nucleation occurred at the boundary of the equilibrium curve for pure CO_2 hydrate (Fig. 2; Adisasmito *et al.* 1991[34]), and that the subsequently observed gas consumption occurred deep within the mixed hydrate regime (Fig. 2; Delahaye *et al.* 2006[13]) leads to the well-founded assumption that indeed primarily mixed species are formed. This hypothesis is further substantiated in relation to the obtained IR-spectroscopic data in the presence of THF (see Section 2.2.2). To which grade pure CO_2 hydrate forms during the remaining time of the experiment remains an open question. However, based on the continuous gas consumption after replenishing gaseous CO_2 (*i.e.*, an increase in pressure to approx. 27 bar; Fig. 1a and b: 3) it is assumed that also pure species are formed, as the system is clearly driven into the pure CO_2 hydrate regime (Fig. 2).

2.2 *In situ* MIR-FEFS monitoring of CO_2 gas hydrates

Next to recording conventional pressure/temperature traces, the main focus of this study was to correlate for the first time such physical observations with molecularly discriminative data on CO_2 gas hydrate formation *via* mid-infrared fiber optic evanescent field spectroscopy (MIR-FEFS). During gas hydrate formation, the present molecules are responsible for specific spectroscopic changes.[30,31] Fig. 3a and b exemplarily display such obtained IR-spectra with and without gas hydrate being present in H_2O (a) and in D_2O (b).

In the MIR spectral regime water (*i.e.*, aqueous species including H_2O and D_2O) is characterized by several distinctive absorption features. The broad absorption band ranging from 3750–2750 cm^{-1} represents the OH stretching vibration (ν_{OH}).
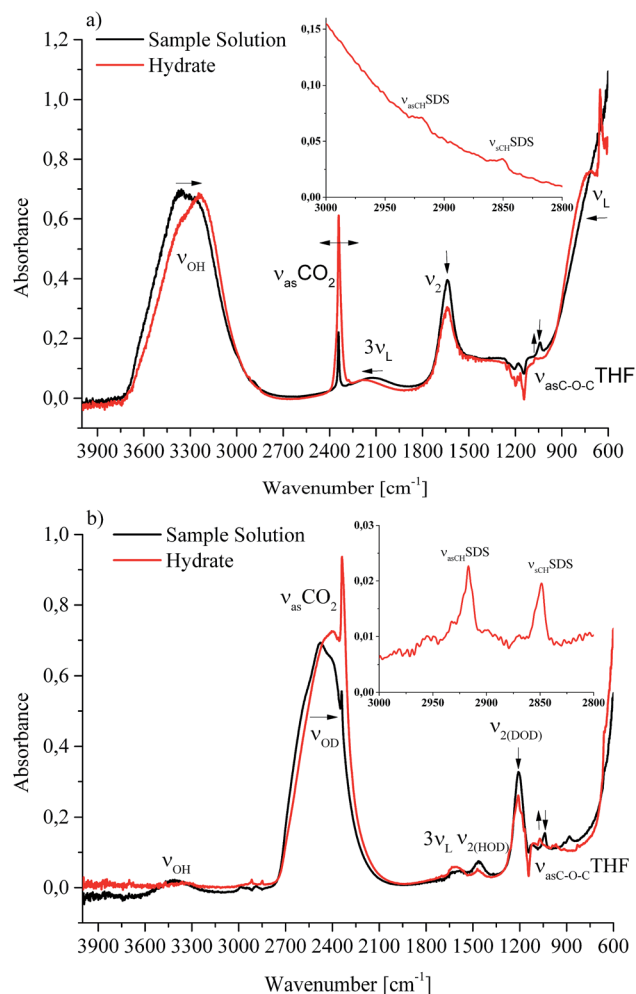

Fig. 3 IR-spectra recorded *in situ via* MIR-FEFS on sample solutions enriched with CO_2 (*i.e.*, the liquid phase with the dissolved gas) in comparison to solid gas hydrate spectra in (a) H_2O and (b) D_2O; the insets magnify the spectral region where SDS provides characteristic IR absorption bands within the hydrate spectra.

Between 2250 and 1950 cm^{-1}, the rather weak 3rd overtone of the libration (3ν_L) mode is evident. The HOH bending vibration ($\nu_{2(HOH)}$) absorbs in the range of 1850–1520 cm^{-1}. Limited by the cut-off frequency of the applied mercury–cadmium–telluride (MCT) detector, the fundamental libration band is just evident <1000 cm^{-1}. Due to the isotopic effect, these absorption features are accordingly shifted to lower wavenumbers for D_2O. The broad ν_{OD} absorption band is evident at 2800–2000 cm^{-1}, and the DOD bending vibration ($\nu_{2(DOD)}$) at 1350–1145 cm^{-1}. The weak absorption feature between 1680 and 1535 cm^{-1} may be assigned to the 3rd overtone of the libration (3ν_L) mode. The libration mode (ν_L) of D_2O is not detectable given the frequency cut-off of the applied detector. Due to the impurities by water/ vapour, the mixed species HDO is ubiquitously present during D_2O experiments, which is evident due to the associated absorption features between 3620 and 3200 cm^{-1} (ν_{OH}), and between 1520 and 1385 cm^{-1} ($\nu_{2(HOD)}$).[35,36] Next to H_2O and D_2O, the used additives THF and SDS also provide specific vibrational absorption features in the MIR. The magnifications of the

obtained MIR-FEFS spectra represent the region of interest for the ν_{asCH}SDS (centered at 2920 cm^{-1} in H$_2$O and 2917 cm^{-1} in D$_2$O), and the ν_{sCH}SDS (centered at 2851 cm^{-1} in H$_2$O and 2849 cm^{-1} in D$_2$O) CH$_2$ bands[37] in the hydrate spectra. For THF, the pronounced asymmetric C–O–C vibration $\nu_{asC-O-C}$THF is evident (centered at 1041 cm^{-1} in H$_2$O and 1039 cm^{-1} in D$_2$O) in the sample spectra.[38] In the region between 1270 and 1100 cm^{-1} absorption features of the used poly(tetrafluoroethylene) (PTFE) ferrules for sealing the IR fiber into the feed-through of the pressure vessel are evident. In the D$_2$O experiment, these are being convoluted by the DOD absorption feature ($\nu_{2(DOD)}$). CO$_2$ is characterized by the strong asymmetric stretching vibration centered at 2342 cm^{-1} in H$_2$O and at 2341 cm^{-1} in D$_2$O (for sample solution spectra), which appears convoluted by the ν_{OD} feature. The ν_{as}CO$_2$ appears substantially increased in the hydrate spectra, which is attributed to the formation of gas hydrate and/or to the increase in dissolved CO$_2$ in the remaining intermediate water phase. A more detailed description of this band is given in Section 2.2.3. During hydrate formation, H$_2$O/D$_2$O associated features are subject to specific changes that are qualitatively similar to the changes occurring during cooling and crystallization of pure water.[39,40] While in the present study these changes are qualitatively similar for both H$_2$O and D$_2$O, they appear more clearly evident during H$_2$O experiments, due to the absence of HOD and other interferences (CO$_2$ and PTFE). While the ν_{OH} (ν_{OD}) features are subject to a red-shift, the $3\nu_L$ and ν_L features shift to the blue. For the bending absorption (i.e., $\nu_{2(HOH)}$ ($\nu_{2(DOD)}$)), the intensity decreases with increased hydrate formation. In general, the evaluation of such features was achieved via peak area integration or peak fitting methods for the different absorption features, respectively. A more detailed description on the evaluation of CO$_2$-containing gas hydrate IR-spectra has been published elsewhere.[41]

The main focus of the present study was to provide further data on spectroscopic changes associated with additives present during the gas hydrate formation. Due to the interference of the IR-signature associated with the water background matrix, D$_2$O was considered as a viable alternative providing a similar chemical environment, yet it facilitates monitoring of these species by the shifted background absorptions of the bulk matrix. As evident in the magnified spectral regime in Fig. 3b, the region of interest for SDS is not convoluted by any water absorbances, which particularly facilitates spectral studies of this system.

2.2.1 The role of SDS during CO$_2$ gas hydrate formation. For hydrocarbon gas hydrates, Luzinova et al. proposed that SDS affects the free propane diffusion gradient, therefore leading to an accelerated gas hydrate formation. Using MIR-FEFS, a significant increase in the peak area associated with the symmetric CH stretch vibration of SDS during gas hydrate formation was detected. However, it was noted that it was not possible to differentiate between SDS micelles, molecular assemblies or small SDS particulates of hydrated solids.[31] Due to the isotopic shift induced by replacing H$_2$O with D$_2$O, the absorption features of SDS are more pronounced in the present studies avoiding convolution with the ν_{OH} absorption feature. In order to further investigate the influence of SDS on CO$_2$-

containing hydrates, the associated symmetric CH absorption feature was evaluated via peak area integration between 2860 and 2842 cm^{-1} (Fig. 4).

The borders of the applied peak area integration method were selected to cover the range of the evolving peak for all spectra in both experiments; the first spectra do not show any signal characteristic for SDS. Gas hydrate nucleation occurred after approx. 2.8 hours in D$_2$O, and after approx. 3 hours in H$_2$O, as evident in Fig. 1. For clarity, this is illustrated by a red line at 2.9 hours in the inset of Fig. 4. The inset in Fig. 4 shows the development of ν_{sCH}SDS during the first 80 hours of the experiments. The peak area for both measurements tends to increase over several hours following nucleation, until reaching equilibrium. For D$_2$O, after approx. 25–30 hours the peak area gradually increases again, which can be correlated to a pressure drop (see Fig. 1). This increase continues until approx. 130 hours, where again a pressure drop occurred. Thereafter, no further increase in the peak area was observed. Thereafter, the pressure was increased two more times, however, with rather slow observable decreases as compared to the previous pressure drops. Hence, the formation process was considered complete or to continue only very slowly. The observed increases and decreases in pressure did not lead to any further detectable changes regarding SDS. In the case of H$_2$O, the gradual increase in peak area was not observed. However, such behaviour is evident in the data between approx. 218 and 230 hours. A decrease in pressure occurred in the corresponding pT trace during that time, after which the pressure was increased once more. The peak area only decreased again upon inducing decomposition of the gas hydrate at the end of the data recording for both experiments. For interpreting the involvement of SDS during gas hydrate nucleation/formation, the attraction of surfactant molecules to the surfaces at the solid/liquid interface is of importance. Since the peak area rises gradually over time during the experiment (in the case of D$_2$O), and since a distinguishable influence via a decrease or increase of pressure appears absent except for the events discussed
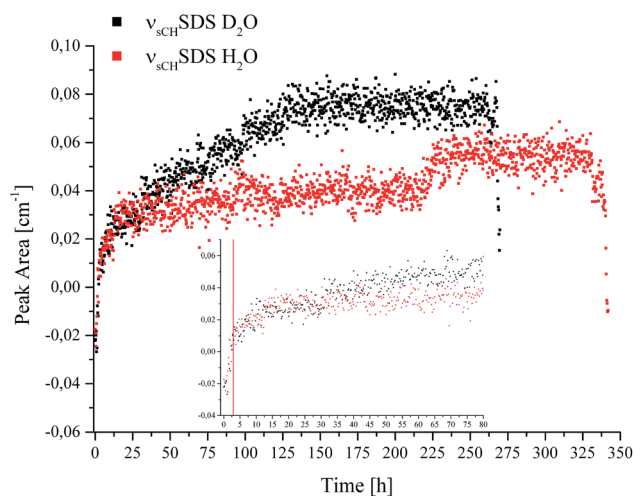

Fig. 4 Peak area of the ν_{sCH}SDS feature vs. time recorded during CO$_2$ hydrate formation in D$_2$O (black) and H$_2$O (red).

above, it is hypothesized that the increase in peak area is likely due to an accumulation of SDS at the waveguide surface. Furthermore, it is known that dodecyl sulphate anions adsorb at the hydrate/liquid interface of THF hydrate particles,[42] which may in turn affect the detection of SDS. An inclusion of SDS molecules in the hydrate cages is unlikely due to the size limitation of the cages.[2] Luzinova *et al.* were able to correlate a sharp rise in the peak area of SDS, and changes of IR water features with the nucleation of gas hydrate at the surface of the fiber.[31] Even though the nucleation of the present experiments started after approx. 2.8/3 hours and a rise in the peak area during the following period was observed, it was not possible attributing this behaviour unanimously to gas hydrate formation at the surface of the fiber, as previous experiments did not reveal sharp instantaneous changes for the spectral features of water simultaneously with the hydrate nucleation,[41] as shown by Luzinova *et al.* Additionally, the concentration of SDS in the present work was considerably higher than in the experiments by Luzinova *et al.*[31] The comparison of the two systems studied so far (*i.e.*, propane gas hydrate and CO_2 gas hydrate) is therefore challenging, as the solubility of CO_2 in water is significantly higher compared to that of short-chained hydrocarbons. Hence, the initially proposed mechanism[31] that SDS increases the transport of gas within the liquid phase is not likely to be applicable for CO_2 gas hydrate formation. Therefore, based on the data obtained herein the question whether SDS leads to the nucleation/formation of gas hydrate in the vicinity of the waveguide surface for CO_2/THF hydrate remains debatable. While the measurement technique used herein is in general highly reproducible, in the specific case of SDS the shape of the molecule-specific absorption features revealed some variance apparently resulting from parameters associated with the hydrate growth.

2.2.2 The role of THF during CO_2 hydrate formation.

During previous studies, the combined application of SDS and THF was used for further promoting hydrate formation.[17–19] Similar to SDS, THF exhibits distinctive absorption features in the MIR (Fig. 3a and b). The strong asymmetric C–O–C stretching vibration is evident in both H_2O and D_2O experiments. Fig. 5 displays the spectral region of interest regarding the asymmetric C–O–C stretch absorption of THF for H_2O and D_2O experiments, each with and without the presence of hydrate.

IR spectroscopic studies on thin films of THF hydrate by Fleyfel and Devlin assigned an absorption feature at 1074 cm^{-1} at 90 K to the asymmetric C–O–C stretch of THF in the large cages of the sII hydrate structure. Furthermore, they observed a doublet of the THF absorption feature at very low temperatures (13 K), which was attributed to THF in two unequal positions within the hexakaidecahedral cages of the hydrate structure.[25] Recent publications observed the feature at 1073 cm^{-1} for a double clathrate hydrate consisting of THF and HCN at 130 K,[43] and at 1073 cm^{-1} for a 90% deuterated THF and HCN binary clathrate hydrate at 170 K.[44] The weak absorption feature centered at 1072 cm^{-1}, which is present in the H_2O hydrate spectrum in Fig. 4 and evident in more detail in Fig. 5, may therefore be attributed to THF in the large cages of the hydrate
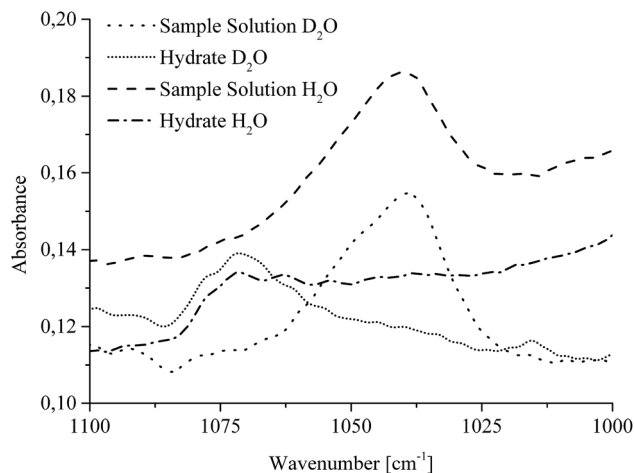

Fig. 5 MIR-FEFS spectra illustrating the spectral shift of the ν_{asCOC}THF absorption band during CO_2 hydrate formation in H_2O and D_2O, respectively.

structure. The minor deviation of the frequency position compared to the literature values is within the spectral resolution (*i.e.*, 2 cm^{-1}) selected for the present study. For the D_2O experiment, the absorption feature of hydrated THF is much more clearly evident (Fig. 3 and 5), which is attributed to the absence of interferences by the ν_L absorption of H_2O in this spectral region (Fig. 5). This observation further consolidates the utility of D_2O facilitating IR spectroscopic investigations on the effects of additives. However, the assignment of this absorption feature to THF inside the clathrate cages remains ambiguous, as the presented data were collected at considerably higher temperatures. A more detailed evaluation of this feature remains limited due to possible influences by spectral features from SDS, which is also present in the solution. The observed species at 1041/1039 cm^{-1} present in the sample spectra of H_2O/ D_2O (Fig. 3 and 5) may be assigned to THF connected with more than three water molecules.[45] To obtain further evidence on the assignment of an enclathrated species, a control experiment with D_2O and only THF as the additive was performed. In the absence of SDS, hydrate growth commences much more slowly[17] without filling the gas hydrate cell even within weeks, in contrast to the presented experiments. In order to provide a more distinct assignment, a pressure cell with a significantly reduced volume is currently developed. Hence, for the purpose of the present study only the THF absorption feature in solution was evaluated. Similar to SDS, the evaluation of the ν_{asCOC}THF-related feature was executed *via* peak area integration between 1058 and 1020 cm^{-1} (Fig. 6).

The inset shows the first 80 hours of the experiments in detail. For comparability, the data was evaluated using the same method for all spectra. The first red line in the inset of Fig. 6 indicates the initiation of nucleation (Fig. 1a and b, in Fig. 6 represented by a single line at 2.9 hours). It is evident that the absorption feature, *i.e.*, the peak area of the non-hydrated THF signal dropped sharply after the first nucleation occurred and continued to decrease with time due to the advancing formation of the hydrate accompanied by the enclathration of THF. The
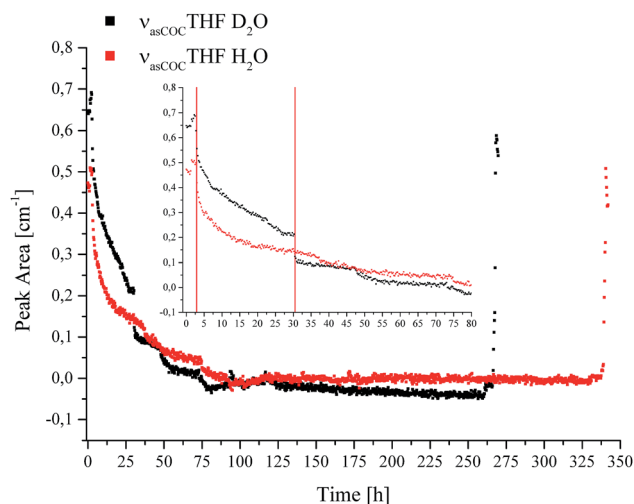
Fig. 6 Peak area for the ν_{asCOC}THF absorption in solution *vs.* time during CO_2 hydrate formation in D_2O (black) and H_2O (red).

resulting structure of the THF/CO_2 hydrate is known as sII with the large cavities occupied by THF, and the small cavities by CO_2.[46] In the case of D_2O another drop is evident at 30.5 hours, indicated by the second red line in the inset of Fig. 6, which can be correlated with a pressure drop (Fig. 1b). The signals of both measurements decrease further until detection is not possible anymore. This implies that there is none or only very little residual THF present in solution in the evanescently probed sampling volume around the fiber after this time. It is assumed that the majority of THF is enclathrated in the hydrate structure at this point. After this point there are still pressure drops evident in the data, which indicate that hydrate formation is not yet completed. Subsequent dissociation of gas hydrate reversed these changes, as anticipated. Torré *et al.* performed CO_2 hydrate experiments under quiescent conditions at various concentrations of THF and SDS, and hypothesized that next to pure CO_2 hydrate a mixed hydrate comprising THF and CO_2 is also formed.[17,18] It should be noted that during the present studies the incorporated gas was discontinuously replenished *via* gas supply several times after the first nucleation occurred ensuring complete formation of gas hydrate within the pressure cell, and especially within the evanescent field surrounding the fiber acting as the ATR-waveguide. The results obtained for THF indicate that the formation of the mixed hydrate in fact commences during the initial phase of the experiment indicated *via* the steadily decreasing peak area for THF in solution. Based on the observation of the absorbance feature of the hydrated THF in Fig. 5, it is assumed that the solid hydrate formed around the fiber consisted of THF and CO_2 with THF being present within the large, and CO_2 within the small cavities of the resulting structure sII. While an undisputable statement on the mechanism of hydrate nucleation cannot be made yet, the applied MIR-FEFS methodology provides a more pronounced sensitivity towards the present additives (*i.e.*, SDS and THF) than any other method reported to date. In the case of water, no distinct changes in the peak area or position could be observed during the initial hydrate formation.[41] An explanation

of this behaviour may be attributed (i) to the presence of considerable amounts of non-hydrated water during the initial formation in the vicinity of the fiber, which renders the detection of structured water species difficult or (ii) based on the interpretation of the obtained results for SDS, that the nucleation is not primarily occurring at the waveguide surface for this system. However, with advancing hydrate formation, spectral changes of water were clearly observed until an equilibrated state was reached (*i.e.*, no further changes were evident in the IR spectra).[41] An explanation for the high efficiency of the combined application of both additives (*i.e.*, THF and SDS) during CO_2 hydrate formation may be the creation of a porous hydrate structure, which in turn leads to a high permeability for CO_2 during the formation.[17] This capillary/pore-based growth mechanism was also proposed for another hydrate system, *i.e.*, gas hydrates of CH_2F_2 with SDS. The authors confirmed that the reaction solution is continuously sucked into the porous hydrate layer at a partially submerged solid interface, which they attributed to the dominating mechanism behind the promoting effect of SDS during hydrate formation.[20] Furthermore, it should be noted that during the present study the existence of micelles is excluded, since the applied concentration of SDS is below the critical micelle concentration (8 mmol L^{-1}).[47] Additionally, the existence of micelles at temperatures below the Krafft point (T_K) of SDS is debatable under hydrate forming conditions.[20,48] In contrast to the studies on SDS, the obtained results for THF appear less affected by the occurring processes and more reproducible from the point of view of molecule-specific spectral characteristics. Yet, common to all executed experiments is a sharp decrease in the peak area after nucleation, evident in the pT – trace along with highly reproducible spectral characteristics for THF.

2.2.3 Monitoring CO_2 during gas hydrate formation. For thin films of CO_2 hydrate, characteristic peaks of the asymmetric stretch vibration for CO_2 molecules in the large ($5^{12}6^2$@2338 cm^{-1}, 135 K) and small (5^{12}@2347 cm^{-1}, 135 K) cages of the structure sI have been reported by Fleyfel and Devlin.[25] Later, Kumar *et al.* applied IR-ATR spectroscopy at −50 °C for identifying characteristic absorption features at 2336 and 2347 cm^{-1} for CO_2 in the large and small cages of the hydrate structure, respectively.[26] During the present study, this type of characteristic peak splitting was not observed, which is predominantly attributed to the significantly higher temperature.[26] Alternatively, it may be hypothesized that the hydrate formed around the fiber consists of THF and CO_2, which would confine the presence of CO_2 to the small cages. However, the expected spectral shift, confirming this assumption (*i.e.*, of the asymmetric stretch to 2346 cm^{-1} at 135 K (ref. 25)) was not observed. The asymmetric stretch of CO_2 is centered at 2341 cm^{-1} in H_2O, and at 2339 cm^{-1} in D_2O in the hydrate spectrum, which is in the range of dissolved gaseous CO_2 (2342.9 cm^{-1} (ref. 49)). Hence, it is not without reason to assume that there is still a considerable amount of CO_2 dissolved in the remaining intermediate water, which leads to this observation. In the D_2O experiment, the absorption feature of CO_2 is convoluted by the strong ν_{OD} stretching absorption, which renders a more detailed evaluation challenging.

3   Experimental

3.1   MIR-FEFS gas hydrate setup

The MIR-FEFS gas hydrate setup comprises four main components: a pressure cell, a FTIR spectrometer, optical coupling components for guiding the IR radiation, and temperature/pressure sensors along with switchable gas/liquid supply connections. Detailed schemes and features of the pressure cell are described elsewhere.[50,51] In brief, the pressure cell provides a fiber feed-through specifically adapted for IR-transparent silver halide fibers enabling *in situ* spectroscopic access to monitoring hydrate formation/dissociation processes. To prevent the silver halide fiber from degradation by contact with base metals the tube fittings of the feed-through are equipped with custom-made PTFE ferrules.[51] Fig. 7 schematically shows the MIR-FEFS gas hydrate setup along with a view into the pressure vessel and the mounted silver halide fiber.

A Bruker IFS/66s model FTIR spectrometer (Bruker Corporation, Billerica, MA, USA) was used during the present studies. The parallel MIR beam was coupled out of the spectrometer and directed *via* a planar 2″ gold coated mirror (Fig. 7 #1) onto a first 90° (2″ focal length) gold-coated off-axis parabolic mirror (OAPM) (Fig. 7 #2), which focuses the radiation onto the facet of the 900 μm diameter silver halide fiber (composition: $AgCl_{0.3}$-$Br_{0.7}$). Inside the fiber, radiation is propagated *via* total internal reflection. After passing the pressure cell (Fig. 7 #3), the emanating light at the distal end of the fiber is collected by a second 2″ 90° OAPM (Fig. 7 #2), and the provided parallel beam is directed onto a third OAPM (Fig. 7 #2) (Edmund Optics Inc., Barrington, NJ, USA) focusing the radiation onto the detector element of a Stirling-cooled mercury–cadmium–telluride (MCT) detector (Model K508, Infrared Associates, Stuart, FL, USA) (Fig. 7 #4). Two optic positioners (Newport Corporation, Irvine, CA, USA) with custom-made PTFE fiber chucks flexibly position the fiber on either side of the pressure cell. Additional parts such as posts and the XYZ translation stage were purchased from Thorlabs Inc (Newton, NJ, USA). The MCT detector was connected to the IFS/66s spectrometer *via* an impedance-matched MCT-1000 pre-amplifier (Infrared Associates, Stuart, Florida USA) *via* an external port. In order to record temperature and pressure traces, the cell was equipped with appropriate sensors mounted at the rear of the pressure vessel: (i) a thermocouple (TEM01.08N.6.0020.T.1KA.0, PKP Prozessmesstechnik, Wiesbaden, Germany) serving as a temperature sensor, and (ii) a stainless steel diaphragm pressure

transducer (AGS4003-60-G-E082, Althen Mess-und Sensortechnik GmbH, Kelkheim, Germany) for pressure tracing. Both were connected to a data logging system (midi LOGGER GL200A, Graphtec, Yokohama, Japan) for directly correlating physical and chemical parameters. Several connectors and drains for liquid and gas supply are implemented on the top and on the rear side of the pressure cell. Gas and liquid connectors are equipped with Swagelok back-pressure valves to avoid leakage (Swagelok, Solon, OH, USA). Cooling of the cell is realized *via* two cooling coils, an internal stainless steel coil (see Fig. 7 view into the pressure vessel), as well as an external copper coil wrapped around the cell. Both coils are connected to a cooling-bath (Lauda RE206, Lauda GmbH & Co. KG, Lauda-Königshofen, Germany) equipped with a thermostat (Lauda E200, Lauda GmbH & Co. KG, Lauda-Königshofen, Germany). To fill the cell with the sample solution, a high performance liquid chromatography pump (HPLC Pump 64, Knauer GmbH, Berlin, Germany) was used. In order to protect the silver halide fiber from degradation,[52] the entire measurement system is surrounded by an acrylic glass box covered with black anodized aluminium foil. To minimize the background fluctuation during the long-term studies, this enclosure is flushed with compressed dry air. IR spectra have been collected every 15 min at a spectral resolution of 2 cm^{-1} between 4000 and 600 cm^{-1} with 500 scans averaged per spectrum. The pT traces have been recorded at intervals of 2 s. For recording and evaluation of the IR spectra, the software packages OPUS 6.5 (Bruker Corporation, Billerica, MA, USA) and Essential FTIR 3.50.047 (Operant LLC, Madison, WI, USA) were used.

3.2   Measurement procedure

The analyzed solution contained 1.5 g L^{-1} SDS and 40 g L^{-1} THF in demineralized water, and was mixed and stirred for approx. 1 hour before use. Demineralized water was replaced by D_2O for the corresponding alternative experiment. Prior to collecting a background spectrum, the box was flushed with dry air for 1.5 hours. Subsequently, the pressure cell was filled with approx. 300 mL of sample solution *via* the HPLC pump system. To remove supernatant air, the cell was purged three times with approx. 10 bar CO_2 and vented down to approx. 3 bar. To obtain a CO_2-enriched solution, the system was then pressurized for 3 hours at approx. 27 bar CO_2 at 20 °C. Pressure, temperature, and IR-spectroscopic data recording were initiated after 2 hours into this initial step. The gas supply was closed after completion of the enrichment step (*i.e.*, 3 hours), and the cooling system was initiated to obtain a temperature of approx. 5 °C. To replenish enclathrated gas in order to entirely fill the cell with hydrate, the gas supply was reopened under pressure several times after the initial nucleation throughout the experiment. The procedure and solution composition have been selected as derived from the literature.[18] Once the absence of a characteristic pressure decrease was determined, the cell was considered filled with hydrates. Dissociation of the hydrate was initiated *via* slow depressurization of the cell by the opening of a bleeding valve. This protocol was applied for all experiments reported herein using H_2O or D_2O as the hydrate matrix. The experiment using
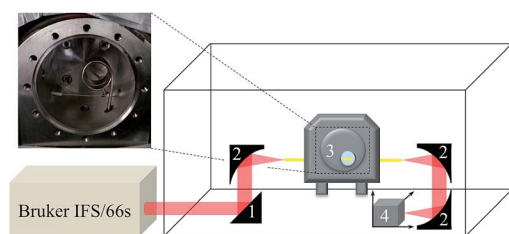

Fig. 7   Schematic of the MIR-FEFS setup and view into the pressure vessel with the mounted silver halide sensing fiber.

H$_2$O as the matrix was independently repeated three times. Using D$_2$O as the matrix, only one experiment was performed, as the only purpose was enabling qualitative insight into the spectral window usually obstructed by water absorption by taking advantage of the isotopic shift within the H$_2$O vs. the D$_2$O spectrum.

3.3 Principles of MIR-FEFS

MIR-FEFS is based on the commonly applied principles of infrared attenuated total reflection (ATR) spectroscopy. In conventional IR-ATR spectroscopy a crystal is used as a waveguide (e.g., ZnSe, Ge, Si, etc.), whereas for FEFS an IR-transparent fiber is applied, here made from polycrystalline silver halides. Propagation of the IR radiation is achieved via total internal reflection in the fiber, which occurs at an interface of an optically denser (n_1) to an optically rarer (n_2) medium at angles exceeding the critical angle Θ_c. At each reflection an evanescent field is induced emanating from the waveguide surface. The penetration depth (d_p) of this field into the surrounding medium is defined as the distance at which the field has decreased to $1/e$ of its initial intensity, and depends on the wavelength (λ), the refractive indices (n_1 and n_2 with $n_2 < n_1$), and the angle of incidence (Θ).[53]

$$\Theta_C = \arcsin \frac{n_2}{n_1}$$

$$d_p = \frac{\lambda}{2\pi \sqrt{n_1{}^2 \sin^2 \Theta - n_2{}^2}}$$

The underlying principles of both techniques (ATR and FEFS) were first introduced by Harrick as internal reflection spectroscopy.[54] Attenuation of the evanescent field by interaction with IR active molecules present within the penetration depth gives rise to the analytical signal. Fig. 8 schematically visualizes a cross-section of the fiber inside the pressure cell surrounded by the measurement solution containing THF, SDS, and CO$_2$.
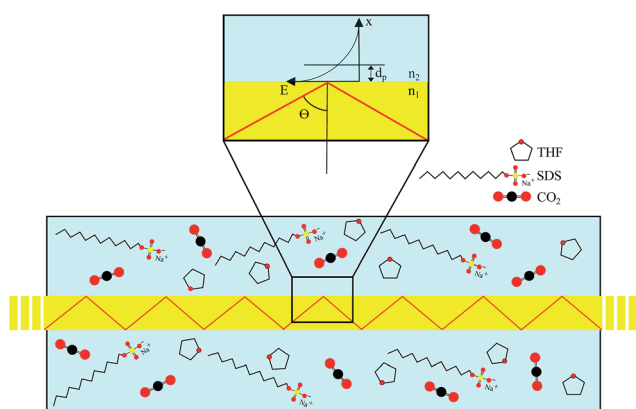

Fig. 8 Principles of MIR–FEFS conceptualized at a cross-section of the scenario within the pressure cell; zoom-in visualizes the exponentially decaying evanescent field emanating from the fiber surface.

3.4 Materials

SDS was purchased from Sigma Aldrich, St. Louis, MO, USA with ≥98.5% purity. THF was purchased from Merck KGaA, Darmstadt, Germany with a purity of ≥99.9%. D$_2$O was purchased from Deutero GmbH, Kastellaun, Germany with 99.9% purity. CO$_2$ gas was purchased from MTI IndustrieGase AG, Neu-Ulm, Germany with 99.8% purity. All chemicals were used as provided and not further purified. The silver halide fiber was fabricated by the team of Abraham Katzir at Tel-Aviv University, Israel.

4 Conclusions

The present study applies for the first time mid-infrared fiber optic evanescent field spectroscopy for in situ studying of CO$_2$ hydrate formation in the presence of various additives. Evidently, insight into complex hydrate formation processes is provided at the molecular-level detail. The spectroscopic evaluation of additives (i.e., THF and SDS) provides additional information for elucidating the promoting effects of these additives during hydrate formation. Finally, studies in D$_2$O as the hydrate-forming matrix assisted in detailing the molecular signatures with yet unprecedented clarity by avoiding the convolution with vibrational absorbances of water in the spectral regions of interest.

The spectroscopic method developed herein enables monitoring gas hydrate formation and dissociation processes associated with additives in situ rendering MIR-FEFS a promising technique for the fundamental investigation of bulk gas hydrates. In the next step, in situ monitoring of the exchange process from CH$_4$ hydrate to CO$_2$ hydrate is anticipated, which is of substantial significance in alternative energy retrieval, energy storage, and carbon capture/sequestration processes. Finally, in-field studies may be envisaged given the current efforts in miniaturizing and harnessing IR-spectroscopic equipment for deep-sea deployment.[53,55]

Acknowledgements

Notes and references

1 E. D. Sloan and C. A. Koh, in Clathrate Hydrates of Natural Gases, CRC Press, Boca Raton, 3rd edn, 2008, ch. 2, p. 45.
2 E. D. Sloan and C. A. Koh, in Clathrate Hydrates of Natural Gases, CRC Press, Boca Raton, 3rd edn, 2008, ch. 2, p. 55.
3 K. A. Udachin, C. I. Ratcliffe and J. A. Ripmeester, J. Phys. Chem. B, 2001, 105, 4200–4204.

4 J. A. Ripmeester and C. I. Ratcliffe, *Energy Fuels*, 1998, **12**, 197–200.

5 F. Qanbari, M. Pooladi-Darvish, S. Hamed Tabatabaie and S. Gerami, *Energy Procedia*, 2011, **4**, 3997–4004.

6 J. Zhao, K. Xu, Y. Song, W. Liu, W. Lam, Y. Liu, K. Xue, Y. Zhu, X. Yu and Q. Li, *Energies*, 2012, **5**, 399–419.

7 H. Komatsu, M. Ota, R. L. Smith and H. Inomata, *J. Taiwan Inst. Chem. Eng.*, 2013, **44**, 517–537.

8 D. Bai, X. Zhang, G. Chen and W. Wang, *Energy Environ. Sci.*, 2012, **5**, 7033–7041.

9 L. C. Elwell and W. S. Grant, *Power*, 2006, **150**, 60–65.

10 P. Linga, R. Kumar and P. Englezos, *J. Hazard. Mater.*, 2007, **149**, 625–629.

11 P. Linga, R. Kumar, J. D. Lee, J. Ripmeester and P. Englezos, *Int. J. Greenhouse Gas Control*, 2010, **4**, 630–637.

12 H. J. Lee, J. D. Lee, P. Linga, P. Englezos, Y. S. Kim, M. S. Lee and Y. D. Kim, *Energy*, 2010, **35**, 2729–2733.

13 A. Delahaye, L. Fournaison, S. Marinhas, I. Chatti, J.-P. Petitet, D. Dalmazzone and W. Fürst, *Ind. Eng. Chem. Res.*, 2006, **45**, 391–397.

14 J.-P. Torré, D. Haillot, S. Rigal, R. de Souza Lima, C. Dicharry and J.-P. Bedecarrats, *Chem. Eng. Sci.*, 2015, **126**, 688–697.

15 K. Okutani, Y. Kuwabara and Y. H. Mori, *Chem. Eng. Sci.*, 2008, **63**, 183–194.

16 Y. Zhong and R. E. Rogers, *Chem. Eng. Sci.*, 2000, **55**, 4175–4187.

17 J.-P. Torré, M. Ricaurte, C. Dicharry and D. Broseta, *Chem. Eng. Sci.*, 2012, **82**, 1–13.

18 J.-P. Torré, C. Dicharry, M. Ricaurte, D. Daniel-David and D. Broseta, *Energy Procedia*, 2011, **4**, 621–628.

19 N. Liu, G. Gong, D. Liu and Y. Xie, *Proceedings of the 6th International Conference on Gas Hydrates (ICGH 2008)*, Vancouver, 2008.

20 K. Watanabe, S. Imai and Y. H. Mori, *Chem. Eng. Sci.*, 2005, **60**, 4846–4857.

21 J. E. Bertie and D. A. Othen, *Can. J. Chem.*, 1972, **50**, 3443–3449.

22 J. E. Bertie and D. A. Othen, *Can. J. Chem.*, 1973, **51**, 1159–1168.

23 J. E. Bertie and J. P. Devlin, *J. Chem. Phys.*, 1983, **78**, 6340–6341.

24 F. Fleyfel and J. P. Devlin, *J. Phys. Chem.*, 1988, **92**, 631–635.

25 F. Fleyfel and J. P. Devlin, *J. Phys. Chem.*, 1991, **95**, 3811–3815.

26 R. Kumar, S. Lang, P. Englezos and J. Ripmeester, *J. Phys. Chem. A*, 2009, **113**, 6308–6313.

27 Y. Jin, H. Oyama and J. Nagao, *Jpn. J. Appl. Phys.*, 2009, **48**, 108001.

28 C. Lo, J. Zhang, P. Somasundaran and J. W. Lee, *J. Colloid Interface Sci.*, 2012, **376**, 173–176.

29 R. Kumar, P. Englezos, I. Moudrakovski and J. A. Ripmeester, *AIChE J.*, 2009, **55**, 1584–1594.

30 G. T. Dobbs, Y. Luzinova, B. Mizaikoff, Y. Raichlin and A. Katzir, *Proceedings of the 6th International Conference on Gas Hydrates (ICGH 2008)*, Vancouver, 2008.

31 Y. Luzinova, G. T. Dobbs, Y. Raichlin, A. Katzir and B. Mizaikoff, *Chem. Eng. Sci.*, 2011, **66**, 5497–5503.

32 A. Klapproth, E. Goreshnik, D. Staykova, H. Klein and W. F. Kuhs, *Can. J. Phys.*, 2003, **81**, 503–518.

33 M. Ricaurte, J.-P. Torré, J. Diaz and C. Dicharry, *Chem. Eng. Res. Des.*, 2014, **92**, 1674–1680.

34 S. Adisasmito, R. J. Frank III and E. D. Sloan Jr, *J. Chem. Eng. Data*, 1991, **36**, 68–71.

35 D. Neubauer, J. Korbmacher, M. Frick, J. Kiss, M. Timmler, P. Dietl, O. H. Wittekindt and B. Mizaikoff, *Anal. Chem.*, 2013, **85**, 4247–4250.

36 J.-J. Max and C. Chapados, *J. Chem. Phys.*, 2002, **116**, 4626–4642.

37 K. V. Padalkar, V. G. Gaikar and V. K. Aswal, *J. Mol. Liq.*, 2009, **144**, 40–49.

38 H. Deng, Z. Shen, L. Li, H. Yin and J. Chen, *J. Appl. Polym. Sci.*, 2014, 40503.

39 J.-B. Brubach, A. Mermet, A. Filabozzi, A. Gerschel and P. Roy, *J. Chem. Phys.*, 2005, **122**, 184509.

40 A. Millo, Y. Raichlin and A. Katzir, *Appl. Spectrosc.*, 2005, **59**, 460–466.

41 M. Schwenk, Y. Raichlin, A. Katzir and B. Mizaikoff, *Proceedings of the 8th International Conference on Gas Hydrates (ICGH8-2014)*, Beijing, 2014.

42 J. S. Zhang, C. Lo, P. Somasundaran, S. Lu, A. Couzis and J. W. Lee, *J. Phys. Chem. C*, 2008, **112**, 12381–12385.

43 I. A. Monreal, L. Cwiklik, B. Jagoda-Cwiklik and J. P. Devlin, *J. Phys. Chem. Lett.*, 2010, **1**, 290–294.

44 N. Uras-Aytemiz, F. M. Balcı, Z. Maşlakcı, H. Özsoy and J. P. Devlin, *J. Phys. Chem. A*, 2015, **119**, 9018–9026.

45 K. Mizuno, Y. Masuda, T. Yamamura, J. Kitamura, H. Ogata, I. Bako, Y. Tamai and T. Yagasaki, *J. Phys. Chem. B*, 2009, **113**, 906–915.

46 M. C. Martínez, D. Dalmazzone, W. Fürst, A. Delahaye and L. Fournaison, *AIChE J.*, 2008, **54**, 1088–1095.

47 D. Rana, G. H. Neale and V. Hornof, *Colloid Polym. Sci.*, 2002, **280**, 775–778.

48 P. Di Profio, S. Arca, R. Germani and G. Savelli, *Chem. Eng. Sci.*, 2005, **60**, 4141–4145.

49 M. Falk and A. G. Miller, *Vib. Spectrosc.*, 1992, **4**, 105–108.

50 N. A. Pennington, Master's Thesis, Georgia Institute of Technology, 2003.

51 G. T. Dobbs, Ph.D. Thesis, Georgia Institute of Technology, 2007.

52 R. Chen, A. Katzir, A. Levite, F. Moser and D. Weiss, *J. Opt. Soc. Am. B*, 1986, **3**, 696–700.

53 B. Mizaikoff, *Meas. Sci. Technol.*, 1999, **10**, 1185–1194.

54 N. J. Harrick, *Internal Reflection Spectroscopy*, Interscience, New York, 1967.

55 M. Kraft, M. Jakusch, M. Karlowatz, A. Katzir and B. Mizaikoff, *Appl. Spectrosc.*, 2003, **57**, 591–599.